

Spectral-based Propagation Schemes for Time-Dependent Quantum Systems with Application to Carbon Nanotubes

Zuojing Chen* and Eric Polizzi†

*Department of Electrical and Computer Engineering,
University of Massachusetts, Amherst, Massachusetts 01003, USA*

(Dated: October 25, 2018)

Abstract

Effective modeling and numerical spectral-based propagation schemes are proposed for addressing the challenges in time-dependent quantum simulations of systems ranging from atoms, molecules, and nanostructures to emerging nanoelectronic devices. While time-dependent Hamiltonian problems can be formally solved by propagating the solutions along tiny simulation time steps, a direct numerical treatment is often considered too computationally demanding. In this paper, however, we propose to go beyond these limitations by introducing high-performance numerical propagation schemes to compute the solution of the time-ordered evolution operator. In addition to the direct Hamiltonian diagonalizations that can be efficiently performed using the new eigenvalue solver FEAST, we have designed a Gaussian propagation scheme and a basis transformed propagation scheme (BTPS) which allow to reduce considerably the simulation times needed by time intervals. It is outlined that BTPS offers the best computational efficiency allowing new perspectives in time-dependent simulations. Finally, these numerical schemes are applied to study the AC response of a (5,5) carbon nanotube within a 3D real-space mesh framework.

PACS numbers: 02.60.x,02.70.Hm,31.15.es

*Electronic address: zuojing@ecs.umass.edu

†Electronic address: polizzi@ecs.umass.edu

I. INTRODUCTION

Nowadays, the numerical solution of the time-dependent Schrödinger-type equation is still considered as one of the most challenging problems in quantum simulations of molecules, nanostructures and devices. In nanoelectronic applications, in particular, efficient time dependent simulations have become increasingly important for characterizing the electron dynamics under time dependent external perturbations such as electromagnetic fields, pulsed lasers, AC signals, particle scattering, etc. For example, THz frequency responses for carbon nanotube (CNT) have recently been observed in [1] pointing out the need of time-dependent simulations capable of going beyond the linear response regime. Reliable modeling approaches in time domain, however, are often limited in term of trade-off between robustness and performances [2, 3].

One approach for solving the time-dependent Schrödinger-type equation consists of using a partial differential equation representation where one can generally discretize the time domain using finite difference method. The specific techniques include both explicit and implicit schemes, with the commonly used Crank-Nicolson scheme [4]. These numerical techniques can be cast as direct approaches, however, they can end up being numerically expensive in the case of long time quantum simulations where it is essential to preserve accuracy and robustness.

Another commonly used approach consists of solving the integral form of the problem via the numerical treatment of the time-ordered evolution operator. Two cases can then be generally considered: (i) The Hamiltonian is time-independent; (ii) The Hamiltonian is time-dependent. In order to solve this latter, one traditional solution consists of dividing the simulation time domain into tiny time steps Δ_t , such that the Hamiltonian can be considered as time-independent within Δ_t and the system can be solved with techniques similar to case (i). Case (i) is indeed formally straightforward, since the problem is then equivalent to solving the exponential of a Hamiltonian. The most obvious way to address this numerical problem would be to directly diagonalize the Hamiltonian while selecting the relevant number of modes (i.e. eigenpairs) needed to accurately expand the solutions. Spectral decomposition, however, are known to be computationally demanding especially for large systems. The mainstream in time dependent simulations has then been to avoid solving directly the eigenvalue problem and use approximations most often based on split operator

techniques [5–7]. In this paper, however, it is pointed out that direct diagonalizations can now be efficiently performed by taking advantage of the recent high-performance eigenvalue solver FEAST [8, 9].

However, when the Hamiltonian is time-dependent, a direct propagation technique still involves solving a very large number of eigenvalue problems along the whole simulation times. Although, the FEAST solver can be used at each time step to speed up the numerical process, we propose here to introduce novel spectral-based propagation schemes that can significantly reduce the total number of eigenvalue problems while preserving high numerical accuracy and robustness. The high-efficiency of these techniques can be achieved, in particular, by considering larger Δ_t and focusing only on obtaining the final states at the end of each time interval.

This paper is organized as follows: Section II presents the basics of time dependent Schrödinger equation within the TDDFT and Kohn-Sham formalism; Section III describes the various propagation approach used in this work including a direct scheme, a novel Gaussian quadrature scheme, and an optimized basis transformed propagation scheme (BTPS); The numerical efficiency of these techniques is finally compared in Section IV using simulation results on 3D CNT.

II. TIME-DEPENDENCE IN QUANTUM SYSTEMS

In quantum systems, the electrons obey the time-dependent Schrödinger equation:

$$i\hbar\frac{\partial}{\partial t}\Psi(t) = \hat{H}\Psi(t). \quad (1)$$

Using a single electron picture, the Hamiltonian is composed of two terms, one of kinetic origin and another describing the interaction of the particle with a local potential which may be time dependent:

$$\hat{H} = \hat{T} + \hat{V}(t) = -\frac{\hbar^2}{2m}\nabla^2 + v(\mathbf{r}, t). \quad (2)$$

Besides appropriate boundary conditions, the time dependent Schrödinger equation requires an initial value condition $\Psi(t = 0) = \Psi_0$ that completely determines the dynamics of the system. In particular, within the time dependent density functional theory (TDDFT) framework [10], the solutions of the stationary Kohn-Sham Schrödinger-type equation are taken as initial wave functions and will be propagated over time.

TDDFT can be viewed as a reformulation of time dependent quantum mechanics where the basic variable is no longer the many body wave function, but the time dependent electron density $n(\mathbf{r}, t)$. For a system composed of N_e electrons, the electron density can be obtained from the solution of a set of one body equations, the so called Kohn Sham equations, that have the same form as Equation (1) where $\Psi = \{\psi_1, \psi_2, \dots, \psi_{N_e}\}$ and with ψ_j solution of:

$$i\hbar \frac{\partial}{\partial t} \psi_j(\mathbf{r}, t) = \left[-\frac{\hbar^2}{2m} \nabla^2 + v_{KS}[n](\mathbf{r}, t) \right] \psi_j(\mathbf{r}, t). \quad (3)$$

The density of the interacting system can be obtained from the time-dependent Kohn-Sham wave functions

$$n(\mathbf{r}, t) = \sum_{j=1}^{N_e} |\psi_j(\mathbf{r}, t)|^2. \quad (4)$$

The Kohn-Sham potential v_{KS} is a functional of the time-dependent density and it is conventionally separated in the following way:

$$v_{KS}[n](\mathbf{r}, t) = v_{ext}(\mathbf{r}, t) + v_H[n](\mathbf{r}, t) + v_{xc}[n](\mathbf{r}, t), \quad (5)$$

where the first term represents the external potential, the second term is the Hartree potential which accounts for the electrostatic interaction between the electrons, and the last term is defined as the exchange-correlation potential which accounts for all the non-trivial many-body effects. Finally, it should be noted that at $t = 0$, the initial wave functions $\Psi_0 = \{\psi_1^{(0)}, \psi_2^{(0)}, \dots, \psi_{N_e}^{(0)}\}$ are solutions of the ground state DFT Kohn-Sham stationary equations [11]:

$$\left[-\frac{\hbar^2}{2m} + v_{KS}[n](\mathbf{r}) \right] \psi_j^{(0)}(\mathbf{r}) = E_j^{(0)} \psi_j^{(0)}(\mathbf{r}). \quad (6)$$

In a confined system, the Kohn-Sham wave function $\psi_j^{(0)}$ (i.e. $\psi_j(\mathbf{r}, t = 0)$) is associated with the eigenvalue $E_j^{(0)}$, and the ground state many-body density is given by $n(\mathbf{r}, t = 0)$. Formally, the solution of Equation (1) can be written as

$$\Psi(t) = \hat{U}(t, 0) \Psi_0 = \mathcal{T} \exp \left\{ -\frac{i}{\hbar} \int_0^t d\tau \hat{H}(\tau) \right\} \Psi_0, \quad (7)$$

where the evolution operator \hat{U} is unitary and can be represented using a time ordered exponential $\mathcal{T} \exp$, which is a non-trivial mathematical object defined in noncommutative algebras. It is important to note that if the Hamiltonian is time-independent, the solution takes a simplified form:

$$\Psi(t) = \exp \left\{ -\frac{i}{\hbar} t \hat{H} \right\} \Psi_0. \quad (8)$$

Unfortunately, this is not the case in most relevant applications which require the description of the electron dynamics under time dependent external perturbations such as electromagnetic fields, pulsed lasers, AC signals, particle scattering, etc. In this case, approximations such as perturbation theory or linear response are commonly used to simplify the computational cost of the time-dependent solutions. In the following Section III, however, novel spectral-based propagation schemes are proposed to address the numerical challenges of solving (7) for the case of large scale problems and long simulation time domains. In order to ease the description of the numerical techniques, one will consider only non-interacting systems (i.e. the potential v is time dependent but it is not a functional of n). The natural extension of these numerical schemes to solving non-linear problems will be discussed in Section V.

III. SPECTRAL-BASED PROPAGATION SCHEMES

A. Direct propagation approach

In practice, intermediate physical solutions are computed in addition to the final solution $\Psi(t)$, in order to describe the evolution of the system over $[0, t]$. This can be accomplished by dividing $[0, t]$ into smaller time intervals since using the intrinsic properties of the evolution operator, one can apply the following decomposition:

$$\hat{U}(t, 0) = \hat{U}(t_n, t_{n-1})\hat{U}(t_{n-1}, t_{n-2}) \dots \hat{U}(t_2, t_1)\hat{U}(t_1, t_0), \quad (9)$$

where we consider $n - 1$ intermediate interval time steps with $t_0 = 0$, and $t_n = t$. Most often a constant time step Δ_t is used and one has to deal now with the problem of performing many shorter time propagation of the solutions along the whole interval $[0, t]$:

$$\Psi(t + \Delta_t) = \mathcal{T} \exp \left\{ -\frac{i}{\hbar} \int_t^{t+\Delta_t} d\tau \hat{H}(\tau) \right\} \Psi(t). \quad (10)$$

Additionally, if Δ_t is chosen very small, it is reasonable to consider $\hat{H}(\tau)$ constant within the time interval $[t, t + \Delta_t]$ leading to

$$\Psi(t + \Delta_t) = \hat{U}(t + \Delta_t, t)\Psi(t) = \exp \left\{ -\frac{i}{\hbar} \Delta_t \hat{H}(t) \right\} \Psi(t), \quad (11)$$

which is also equivalent to solving the time independent problem (8).

Denoting \mathbf{H} the $N \times N$ Hamiltonian matrix obtained after the discretization of \hat{H} at a given time t and where N could represent the number of basis functions (or number of nodes using real-space mesh techniques), \mathbf{H} can then be diagonalized as follows:

$$\mathbf{D} = \mathbf{P}^T \mathbf{H} \mathbf{P}, \quad (12)$$

where the columns of the matrix $\mathbf{P} = \{\mathbf{p}_1, \mathbf{p}_2, \dots, \mathbf{p}_M\}$ represent the eigenvectors of \mathbf{H} associated with the M lowest eigenvalues regrouped within the diagonal matrix $\mathbf{D} = \{d_1, d_2, \dots, d_M\}$. If the discretization is performed using non-orthogonal basis functions (e.g. finite element basis functions in real-space), the eigenvalue problem that needs to be solved takes the generalized form:

$$\mathbf{H} \mathbf{p}_i = d_i \mathbf{S} \mathbf{p}_i, \quad (13)$$

where \mathbf{S} is a symmetric positive-definite matrix. Here, we consider that the computed eigenvectors \mathbf{P} are \mathbf{S} -orthonormal i.e. $\mathbf{P}^T \mathbf{S} \mathbf{P} = \mathbf{I}$. In order to evaluate the exponential of the Hamiltonian in (11), it is now possible to perform a spectral decomposition where the exponential acts only on the eigenvalue matrix \mathbf{D} . One can show that the resulting matrix form of time propagation equation is given by:

$$\Psi(t + \Delta t) = \mathbf{P} \exp \left\{ -\frac{i}{\hbar} \Delta t \mathbf{D} \right\} \mathbf{P}^T \mathbf{S} \Psi(t), \quad (14)$$

which is exact if $M = N$. We also note that $\Psi^T \mathbf{S} \Psi = \mathbf{I}$ with $\Psi = \{\psi_1, \psi_2, \dots, \psi_{N_e}\}$. In practice, it is reasonable to obtain very accurate spectral approximations even if one selects the number of lowest eigenvalues M much smaller than the size of the system N but greater than N_e (i.e. $N_e < M \ll N$). The N_e propagating states Ψ are indeed low energy states. In this case, Ψ , \mathbf{P} , \mathbf{D} , \mathbf{S} are respectively matrices of size $N \times N_e$, $N \times M$, $M \times M$, and $N \times N$. Using the property (9), the solution $\Psi(t)$ can finally be obtained in function of Ψ_0 :

$$\Psi(t) = \mathcal{T} \left\{ \prod_i \left[\mathbf{P}_i \exp \left(-\frac{i}{\hbar} \Delta t \mathbf{D}_i \right) \mathbf{P}_i^T \mathbf{S} \right] \right\} \Psi_0, \quad (15)$$

where $\mathbf{D}_i = \mathbf{P}_i^T \mathbf{H}(t_i) \mathbf{P}_i$, and the time ordering is defined by

$$\mathcal{T} \left\{ \prod_i A(t_i) \right\} = A(t_N) \dots A(t_2) A(t_1). \quad (16)$$

Therefore, the direct approach may require solving hundred to thousand of eigenvalue problems all along the time domain (one eigenvalue problem for each time step). For large-scale systems (e.g. where hundreds of atoms are taken into consideration), this approach

is often considered not applicable as accurate eigensolutions for thousands of eigenpairs are computationally demanding and algorithmically challenging. Recently, however, the new density-matrix based algorithm FEAST [8] has been proposed to overcome these difficulties, and provide both accuracy, robustness and performance scalability for solving eigenvalue problems. FEAST is a general purpose algorithm which takes its inspiration from the density-matrix representation and contour integration technique in quantum mechanics. Its main computational tasks consist of solving very few independent linear systems (typically eight linear systems that can be solved simultaneously in parallel) and one reduced dense eigenvalue problem orders of magnitude smaller than the original one (of size $M \times M$, in the present case). FEAST is also ideally suited for the direct propagation scheme presented here, since it can take advantage of the subspace computed at a given time step i as initial guess for the next time step $i + 1$ in order to speed-up the numerical convergence. Ultimately, one can show that if enough parallel computing power is available at hand, the main computational cost of FEAST for solving the eigenvalue problem can be reduced to solving only one linear system. In contrast to the proposed FEAST approach for the direct spectral-based propagation scheme, PDE-based numerical schemes for solving (7) (such as Crank-Nicolson) would require solving successively a large number of linear systems by tiny time intervals Δ_t . A high-performance implementation of the FEAST algorithm can be found in [9].

B. Gaussian propagation scheme

The direct approach has a sounded physical interpretation as it corresponds to a step by step propagation of the solution over time. Its major drawback, however, is that it involves a very large number of time steps from initial to final simulation times. Let us now consider the case of a much greater time interval Δ_t which may correspond, for instance, to a given period of an external time-dependent perturbation. The solution can then be obtained by performing first a numerical integration for the integral on the Hamiltonian in (10):

$$\Psi(t + \Delta_t) = \mathcal{T} \exp \left\{ -\frac{i}{\hbar} \xi \sum_{i=1}^p \omega_i \hat{H}(t_i) \right\} \Psi(t) \quad (17)$$

where ω_i and ξ are integration constant, and p is the number of quadrature points. If the quadrature points are close enough, one can additionally assume that the anti-commutation error between Hamiltonians can be ignored, and the exponential can then be decomposed

into a product of exponentials for each time step

$$\Psi(t + \Delta_t) = \mathcal{T} \left\{ \prod_{i=1}^p \exp \left\{ -\frac{i}{\hbar} \xi \omega_i \hat{H}(t_i) \right\} \right\} \Psi(t). \quad (18)$$

The number of exponentials to evaluate along $[0, t]$ is then equal to the number of time interval n multiply by the number of quadrature points p by intervals. After discretization and spectral decomposition of each Hamiltonian as presented in Section III A, it comes:

$$\Psi(t + \Delta_t) = \mathcal{T} \left\{ \prod_{i=1}^p \left[\mathbf{P}_i \exp \left(-\frac{i}{\hbar} \xi \omega_i \mathbf{D}_i \right) \mathbf{P}_i^T \mathbf{S} \right] \right\} \Psi(t). \quad (19)$$

We note from the derivation of equations (17) and (18) that two numerical errors are respectively involved: (i) an integration error and (ii) an error on the anti-commutation resulting from the decomposition of the exponential. The direct propagation scheme presented in Section III A can be derived by assuming a rectangle quadrature rule with $\omega_i = 1$ and using $\xi = \delta_t$, $t_i = t + (i - 1) * \delta_t$ where $\delta_t \equiv \Delta_t / (p - 1)$ corresponds to a very small time step within intervals. Using this less conventional derivation, it is possible to point out that a drastic reduction of the integration error (17) could be obtained by considering higher-order quadrature scheme such as Gaussian quadrature. A p -point Gaussian quadrature rule is a numerical integration constructed to yield an exact result for polynomials of degree $2p - 1$ by a suitable choice of the points t_i and (Gauss-Legendre) weights ω_i . We associate the quadrature points t_i at the Gauss node x_i using $t_i = \frac{\Delta_t}{2} x_i + \frac{2t + \Delta_t}{2}$, also we note $\xi = \Delta_t / 2$. Gaussian quadrature can use relatively much fewer points than low-order quadrature rule such as rectangle, to yield a high order approximation of the integral of a function. Interestingly, a large number of numerical experiments have shown that accurate exponential decomposition (18) can still be obtained while using much fewer points p or larger spacing within intervals (even in the presence of strong perturbations). The same experiments have demonstrated, however, that increasing the accuracy on the numerical integration plays an important role for obtaining the correct solutions. We will show in Section IV that the Gaussian quadrature scheme provides a good combination of reduced computational consumption and high numerical accuracy. The number of exponentials that needs to be evaluated by time intervals can indeed be reduced by a factor 3 to 4 as compared to the direct approach. Using the Gaussian quadrature, however, the intermediate solutions obtained by propagating the solutions within the intervals have no physical meaning. Since

the quadrature weights ω_i are different for each Gauss node, the solutions can indeed only be known at the beginning and at the end of each interval.

C. Basis transform propagation scheme (BTPS)

By focusing on obtaining only the final states at the end of each time interval Δ_t , the Gaussian propagation schemes can considerably reduce the number of eigenvalue problems that needs to be solved. Yet, solving large scale eigenvalue problems is still the most computational consuming part in our simulation. Here, we introduce a basis transform propagation scheme (BTPS) which can help in reducing not only the number of eigenvalue problems to solve by intervals, but also the size of each eigenvalue problem.

Before performing the decomposition of the exponential, let us first consider the discretization of equation (17):

$$\Psi(t + \Delta_t) = \mathcal{T} \exp \left\{ -\frac{i}{\hbar} \xi \sum_{i=1}^p \omega_i \mathbf{H}_i \right\} \Psi(t), \quad (20)$$

where $\mathbf{H}_i \equiv \mathbf{H}(t_i)$. We propose then to project the ‘‘pseudo-Hamiltonians’’ $\omega_i \mathbf{H}_i$ onto a common eigen-subspace \mathbf{P} constructed from the result of the quadrature sum $\sum_{i=1}^p \omega_i \mathbf{H}_i$. Denoting \mathbf{H} this new ‘‘global Hamiltonian’’ which takes the overall contribution of the time-dependent perturbation over a given time interval Δ_t (however \mathbf{H} has no physical meaning), one can perform the diagonalization defined in (12) i.e.

$$\mathbf{D} = \mathbf{P}^T \mathbf{H} \mathbf{P} \equiv \mathbf{P}^T \left\{ \sum_{i=1}^p \omega_i \mathbf{H}_i \right\} \mathbf{P}, \quad (21)$$

where the subspace \mathbf{P} and eigenvalues \mathbf{D} are obtained solving the eigenvalue problem in (13). Denoting \mathbf{h}_i the projection of the pseudo-Hamiltonians at a given quadrature point such that

$$\mathbf{h}_i = \mathbf{P}^T (\omega_i \mathbf{H}_i) \mathbf{P}, \quad (22)$$

it comes with (21)

$$\mathbf{D} = \sum_{i=1}^p \mathbf{h}_i, \quad (23)$$

where \mathbf{h}_i are $M \times M$ dense matrices while their summation \mathbf{D} is diagonal. Using a spectral decomposition on the time-ordered exponential for the global Hamiltonian, the expression

(20) can now take the following form:

$$\Psi(t + \Delta_t) = \mathbf{P}\mathcal{T} \exp \left\{ -\frac{i}{\hbar} \xi \sum_{i=1}^p \mathbf{h}_i \right\} \mathbf{P}^T \mathbf{S} \Psi(t), \quad (24)$$

where \mathbf{P} has been moved outside the expression of the time-ordered exponential since it is a common subspace for all different quadrature time points within $[t, t + \Delta_t]$. It is then important to note that one cannot replace directly the sum of the projected Hamiltonian in the exponential by \mathbf{D} (23), as the time-ordered operator can only be resolved using a product of functions taken at different times (16). Similarly to the derivation of (18), we assume that the quadrature points are close enough that one can decompose the exponential into a product of exponentials for each time step:

$$\Psi(t + \Delta_t) = \mathbf{P}\mathcal{T} \left\{ \prod_{i=1}^p \exp \left\{ -\frac{i}{\hbar} \xi \mathbf{h}_i \right\} \right\} \mathbf{P}^T \mathbf{S} \Psi(t), \quad (25)$$

Thereafter, one can perform the diagonalization of each \mathbf{h}_i matrices

$$\mathbf{h}_i = \mathbf{q}_i^T \mathbf{e}_i \mathbf{q}_i, \quad (26)$$

where the $M \times M$ matrices \mathbf{q}_i represent the eigenvectors of \mathbf{h}_i , and the diagonal matrices \mathbf{e}_i regroup the associated M eigenvalues. In contrast to the generalized eigenvalue problem on the global Hamiltonian above, these eigenvalue problems are standard i.e.: $\mathbf{h}\mathbf{q} = \mathbf{q}\mathbf{e}$. Finally using a spectral decomposition on the exponentials in (25), we obtain:

$$\Psi(t + \Delta_t) = \mathbf{P}\mathcal{T} \left\{ \prod_{i=1}^p \left[\mathbf{q}_i \exp \left(-\frac{i}{\hbar} \xi \mathbf{e}_i \right) \mathbf{q}_i^T \right] \right\} \mathbf{P}^T \mathbf{S} \Psi(t). \quad (27)$$

In contrast to the propagation schemes presented in Sections III A and III B which required solving $n * p$ large scale eigenvalue problems of size $N \times N$ along $[0, t]$ (n number of intervals Δ_t , and p number of quadrature points), the BTPS approach consists of solving only one $N \times N$ eigenvalue problem by time intervals (21), and $n * p$ reduced dense eigenvalue problems of size $M \times M$ (26).

The values of ξ , t_i and ω_i have been specified in Section III B in the case of a rectangle and Gaussian quadrature rules. We recall that the Gaussian scheme has been proposed to reduce the number of quadrature points p (i.e. number of exponential to evaluate) within interval. From equation (24), however, one can see that the numerical integration is here actually performed on the reduced projected Hamiltonians, and this basis transformation

is expected to significantly decrease the integration error. As a result, we have found that the rectangle quadrature rule is likely to provide the same accuracy than the Gaussian scheme using the same number of quadrature points p . Since this latter cannot be reduced below a certain threshold in order to limit the error arising from the decomposition on the exponentials (25), a high-order integration scheme such as Gauss quadrature becomes then obsolete using BTPS. Similarly the Gaussian scheme, however, intermediate solutions that can be obtained by introducing $\mathbf{I} = \mathbf{P}^T \mathbf{S} \mathbf{P}$ within the product expression in (27), would end up having no physical meaning. Indeed, one can demonstrate that using BTPS the (S)-orthonormalization of the wave functions is only satisfied between the solutions taken at the beginning and at the end of each interval.

IV. SIMULATION RESULTS

We propose to perform time-dependent 3D simulations of an isolated carbon nanotube (CNT) which is sandwiched between two electrodes producing a AC voltage at the THz frequency. In this model, the charge transfer at the contacts is not considered (i.e. open systems and transport problems are not considered). Here, our model uses a local empirical pseudopotential approach, real-space mesh techniques for discretization (finite element method), and a time-dependent version of the atomistic mode approach described in [12, 13]. Moreover, the empirical pseudopotential U_{eps} is supposed time-independent the total atomistic potential can then be decomposed as follows:

$$U(x, y, z, t) = U_{eps}(x, y, z) + U_{ext}(x) \sin(\omega t), \quad (28a)$$

$$U_{ext}(x) = \frac{2x - L}{L} U_0, \quad (28b)$$

where x is the longitudinal direction of the tube, L represents the distance between contacts ($x \in [0, L]$), $\omega = 2\pi f$, with f the corresponding frequency of the AC signal and U_0 its amplitude. The time-dependent external potential applied to the CNT, maintains then zero in the middle of the tube but oscillates at both ends alternatively to the $\pm U_0$ values.

Here, the system under consideration is a 6-unit cell of a (5,5) CNT where the contact-contact distance is set at $1.98nm$. This CNT is composed by 120 atoms, and using the empirical pseudopotential for Carbon atom proposed in [14], one can expect to capture all the 60 electrons (without spin-dependence) contained in the π_z orbitals. Using the notations

defined in Section III, it comes $N_e = 60$, and $M = 120$ (M being the number of eigenpairs used for the spectral decomposition and chosen here as twice the number of electrons N_e). The finite element discretization of the full 3D system gives rise to sparse matrices of size $N \sim 500 * 10^3$, while this size can be drastically reduced in our case using a mode approach in real-space to $N \sim 15 * 10^3$. For the external perturbation (AC signal), we consider $U_0 = 5eV$ and $f = 200THz$. In our simulation, the solution wave functions $\Psi = \{\psi_1, \psi_2, \dots, \psi_{N_e}\}$ will be propagated from $t = 0$ to $t = 8T$ where $T = 1/f = 5 * 10^{-15}s$ denotes the period of the AC signal. The time interval used is $\Delta_t = T$ where we have found that $p = 120$ integration points by intervals are sufficient for the direct propagation scheme to provide an accurate reference solution. Let us recall that direct scheme allows to capture the evolution of all the wave functions at each tiny time step Δ_t/p , while the Gaussian and BTPS approaches are expected to produce only accurate results at each time interval Δ_t which length has been arbitrarily chosen very large here to point out the robustness of the approaches.

In order to examine the relative accuracy and robustness of the numerical techniques presented in this article, we propose to calculate the energy evolution of the wave functions i.e.

$$E_j(t) = \langle \psi_j(t) | \mathbf{H}(t) | \psi_j(t) \rangle, \quad j = 1, \dots, N_e. \quad (29)$$

Let us first discuss the integration error which is introduced in our model in (17). As an example, Figure 1 compares the direct and Gaussian propagation schemes by representing the energy evolution of both the first energy level E_1 and the HOMO level of the system E_{60} . Using a direct scheme with $p = 40$ integration points for performing the rectangle quadrature between time intervals and as compared to the reference curves obtained for $p = 120$, one can see that the results start diverging after few time steps. In contrast to the direct scheme, accurate results can still be obtained at the end of each time period using $p = 40$ and higher order integration technique such as our proposed Gaussian scheme. In practice, Gauss quadrature could accurately perform the numerical integration (17) using much fewer integration points ($p < 40$), however, this would also increase the anti-commutation error arising from the decomposition of the exponential in (18) as discussed in Section III B and shown in Figure 2.

Finally, similarly to the Gaussian propagation scheme, $p = 40$ integration points suffice for the BTPS approach to accurately obtain all the solutions at the end of each time period. Using BTPS the numerical integration is performed on a projected space, and this operation

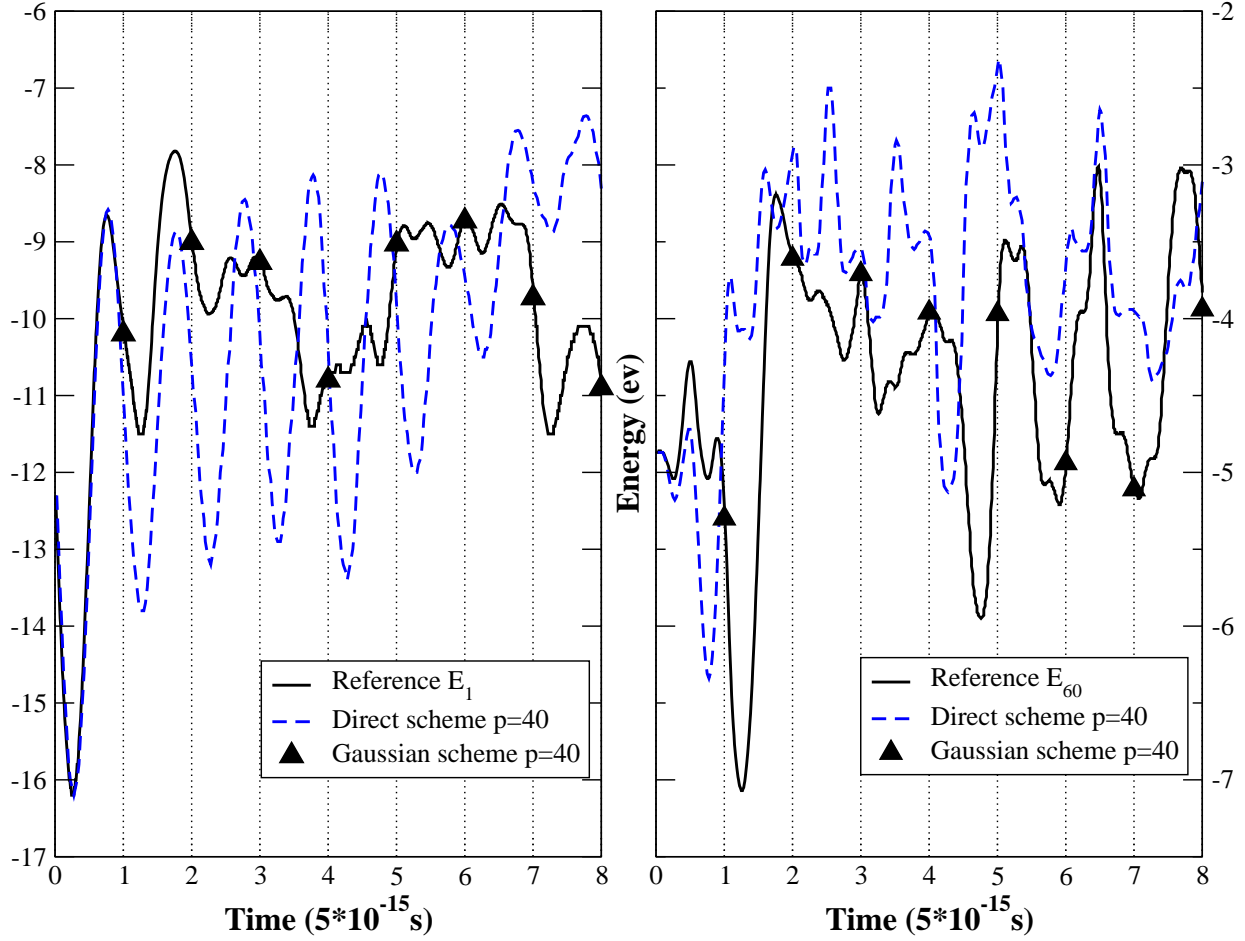


FIG. 1: Evolution of the energy expectation of the first level (on the left) and the HOMO level (on the right) along 8 time periods of the AC signal. The straight lines represent the reference solutions calculated using the direct scheme with $p = 120$ rectangle quadrature points within intervals. The results for the energy evolution using a direct scheme $p = 40$, represented using dashed lines, diverges after few time steps, while the same number of points did suffice for the Gaussian scheme to accurately capture the solutions at the end of each time period (represented by filled triangle symbols).

does not require high-order integration schemes as discussed in Section III C. As compared to direct or Gaussian propagation schemes, BTPS reduces drastically the computational costs meanwhile stable and accurate. However and as shown in Figure 3, intermediate solutions that can be computed within the intervals have no physical meaning. It should be noted that the same remark applied to the Gaussian scheme, although the (unphysical) solutions

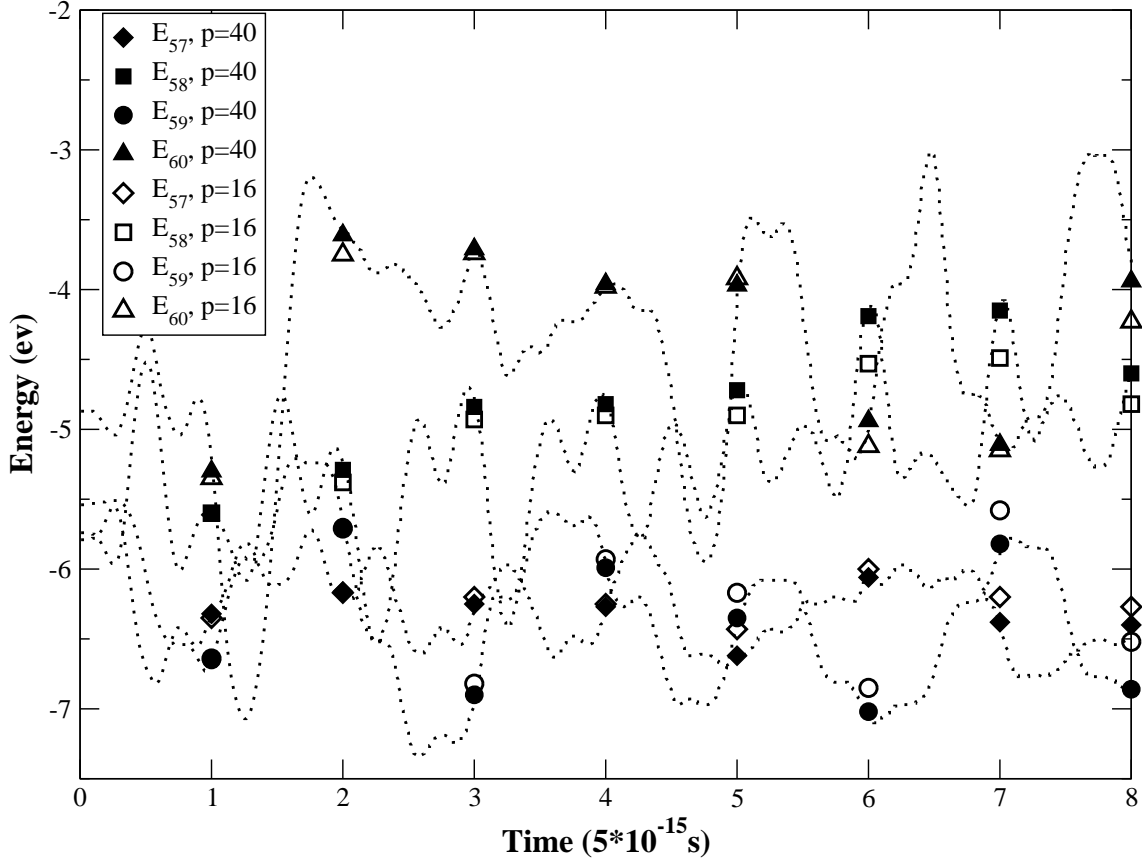


FIG. 2: Evolution of the energy expectation the levels 57 to 60. The filled symbols are obtained using $p = 40$ Gaussian propagation scheme, and match exactly the reference solutions (dashed lines) at the end of each time period. In contrast, the solutions obtained using the $p = 16$ Gaussian scheme, represented by the unfilled symbols, suffer now from an unsuitable approximation on the decomposition of the exponential (18) due to an increase in distance between integration points.

within intervals were not represented in Figures 1 and 2 for clarity.

From the solutions on the wave functions, one can now investigate many properties of the CNT. In particular, within the real-space mesh framework, the electron density is given by:

$$\mathbf{n}(t) = \sum_{j=1}^{N_e} |\psi_j(t)|^2. \quad (30)$$

As an example, the results of the 3D simulations on the electron density are represented in Figures 4 and 5 respectively at $t = 0$ and $t = T/4$ using a contour plot.

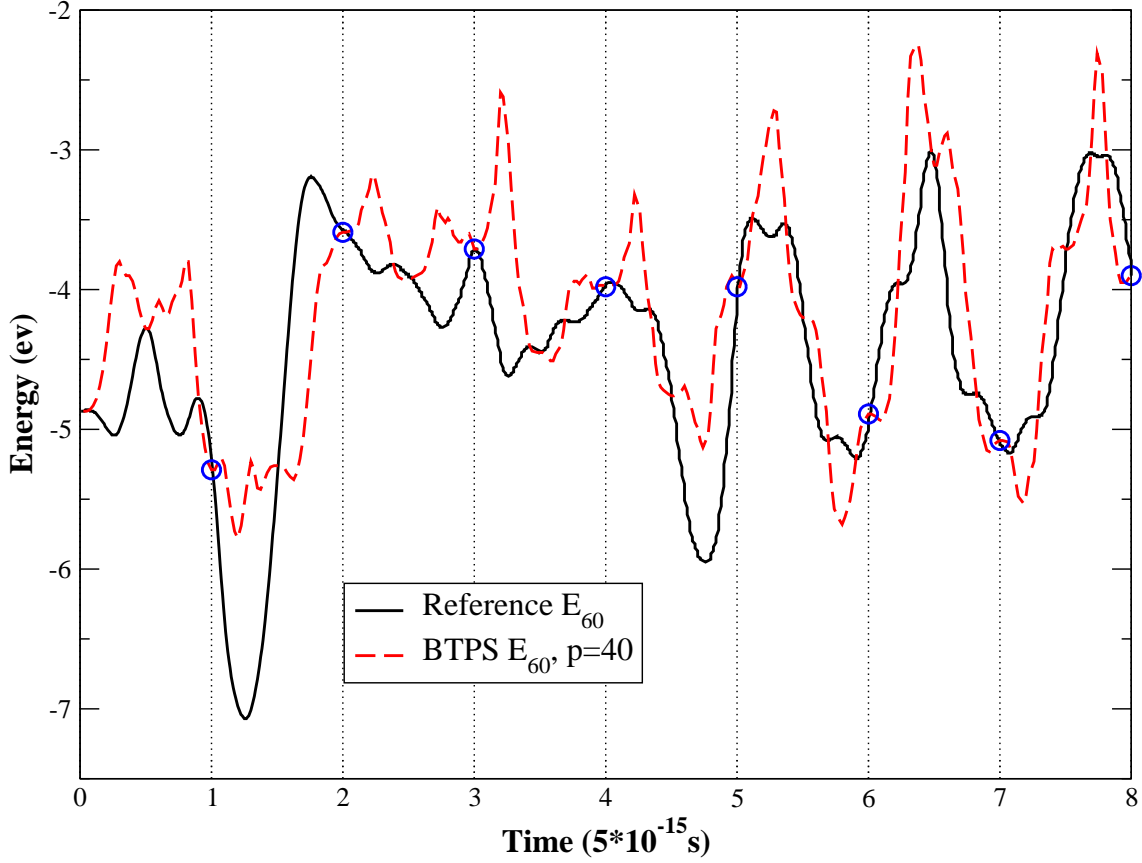


FIG. 3: Evolution of the energy expectation for the HOMO level. BTPS can capture efficiently and exactly the reference solution at the end of each time interval using $p = 40$ points for the rectangle quadrature rule (the BTPS solutions are pointed out in the plot using the circle symbols). We note that the intermediate solutions obtained with BTPS have no physical meaning.

In order to better illustrate the time evolution of the density, it is possible to calculate the variation of the 1D projection of the electron density on the longitudinal axis i.e. $n_{1D}(x) = \int_{y,z} n(x, y, z, t) dy dz$. Figure 6 shows how this 1D electron density calculated using the direct propagation scheme and at some particular positions along x , evolves over time. It should be then noted that much fewer points that the $p = 120$ required by Δ_t using the direct approach, could obviously be sufficient to accurately capture the variation on the density. Indeed, the electron density as well as other integrated quantities, are likely to exhibit much weaker variations as compared to the variations of the individual wave functions. Let us then suppose that the variation of the electron density can be captured using (at most) 30 points

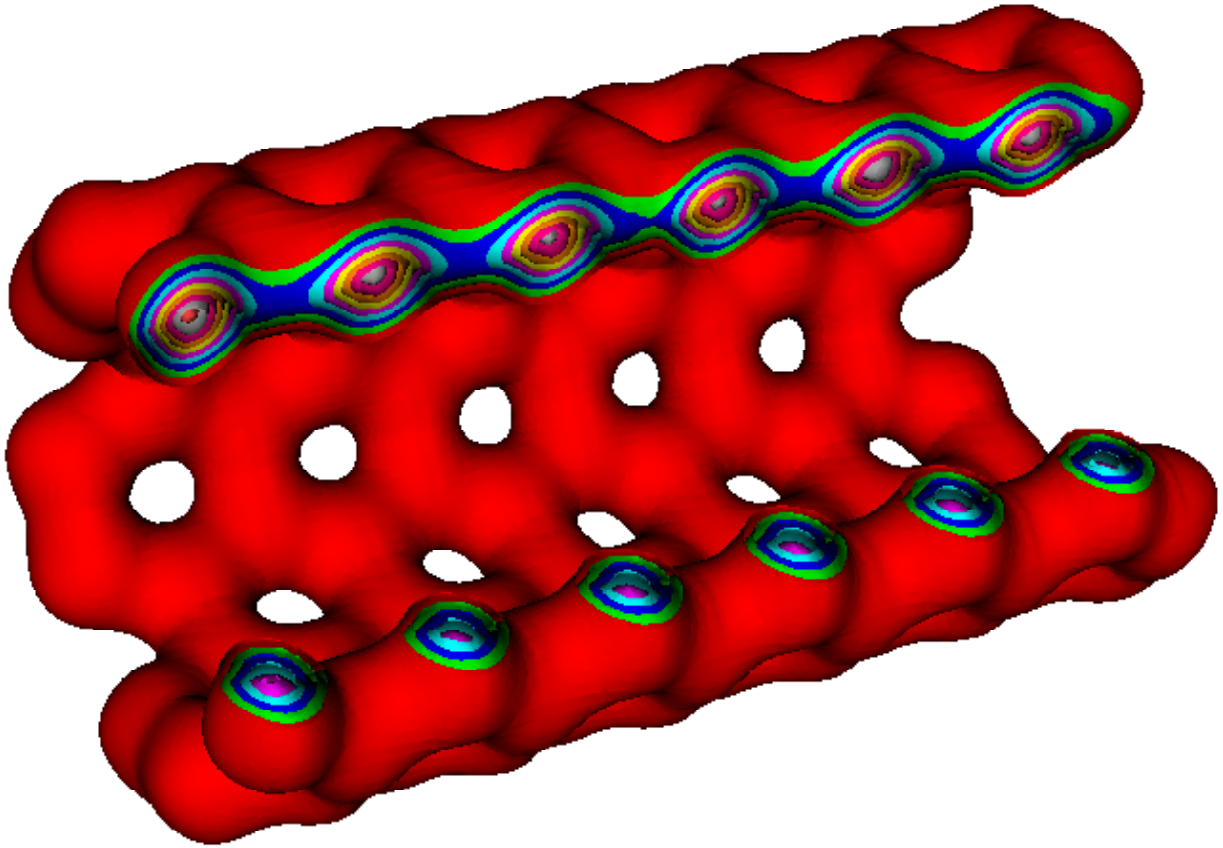


FIG. 4: Contour plot showing the 3D electron density at $t = 0$.

by $\Delta_t = T$, BTPS could then be efficiently used to compute these intermediate solutions using a new time interval of $\Delta_t = T/30$. For the same degree of accuracy, indeed, the direct propagation scheme would now require solving 4 (120/30) large eigenvalue problems within the new Δ_t , but BTPS would still require solving only one (and $40/30 \simeq 1$ small reduced eigenvalue problem).

V. CONCLUSION

In this work, we have investigated three different spectral-based propagation techniques for time dependent quantum system: Direct, Gaussian and BTPS approaches. These numerical schemes have been applied to study the AC response of an isolated single wall carbon nanotube using a real-space mesh techniques framework, empirical pseudopotential and non-interacting TDDFT calculations. Using the direct approach, the time-ordered evo-

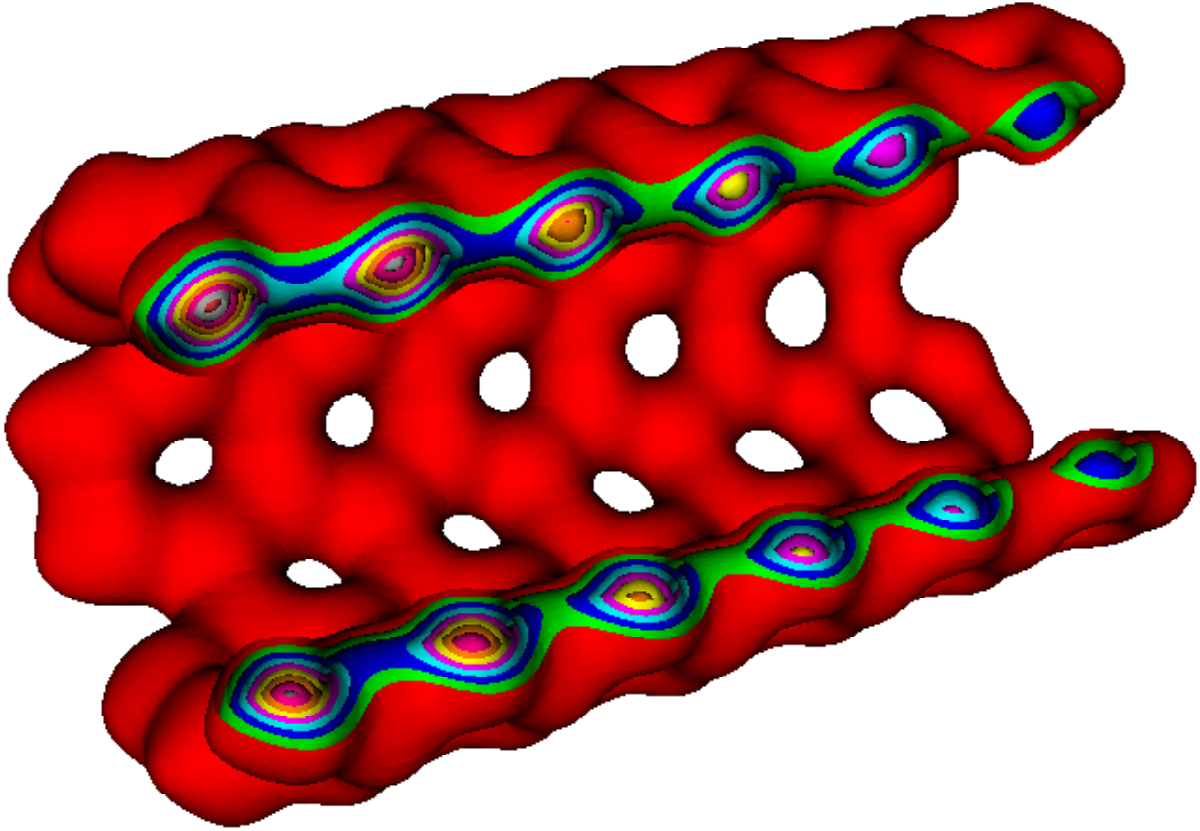


FIG. 5: Contour plot showing the 3D electron density at $t = T/4$, electrons have moved to the left edge.

lution operator is solved via a step-by-step diagonalization procedure of the time-dependent Hamiltonian. Spectral-based schemes are known as robust and accurate but are traditionally considered too computationally expensive for addressing large systems. The new eigenvalue solver FEAST, however, can efficiently address these problems and provide performances and scalability. We have also pointed out that two numerical errors do appear in time propagation problems: a quadrature error resulting from the integral on the Hamiltonian, and an error resulting from the decomposition of the exponential. In contrast to the more conventional direct approach, our proposed Gaussian scheme demonstrates that it is possible to obtain the solutions at the end of each time interval using a reduced number of quadrature points (i.e. reduction of the quadrature error using a higher-order integration scheme), while preserving accurate exponential decompositions. Finally the BTPS scheme reduces not only the number of eigenvalue problems to solve by intervals, but also the size of each eigenvalue

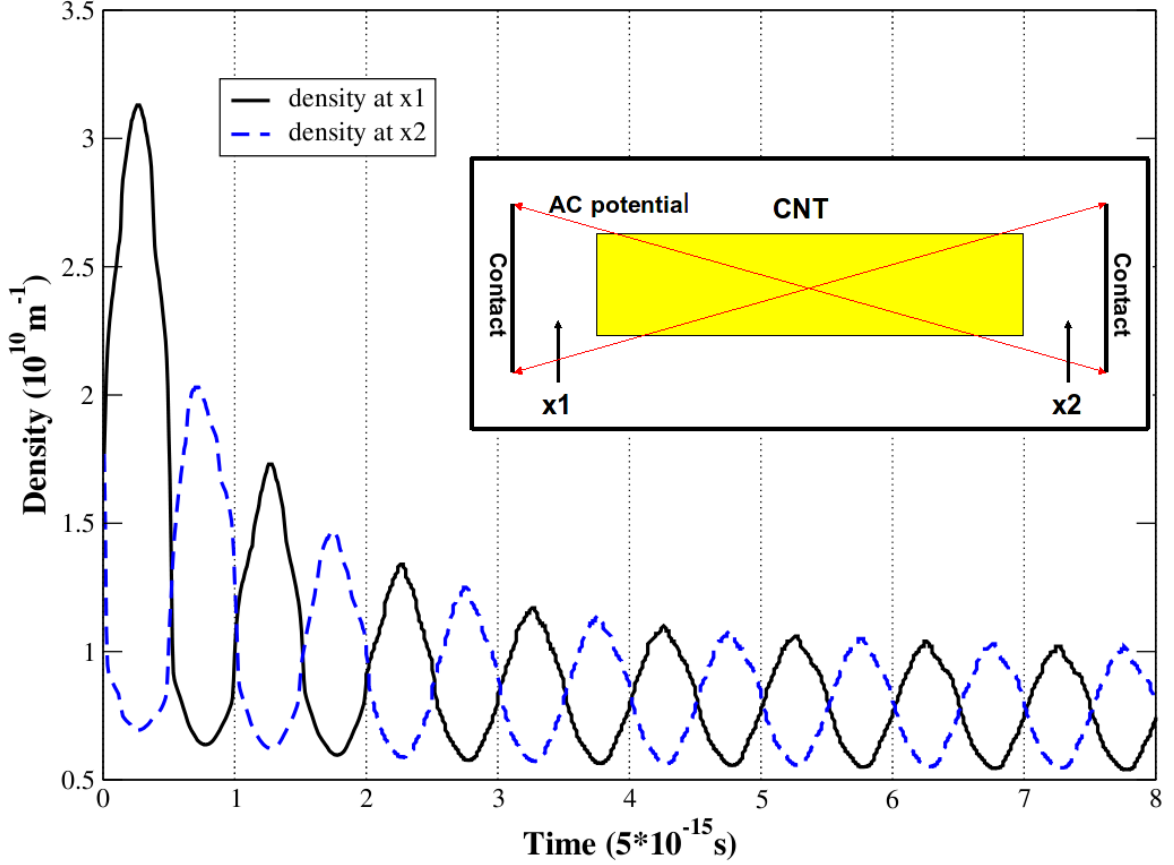


FIG. 6: Evolution of the 1D projection of the electron density at two given positions. In this example, the positions x_1 and x_2 are selected between contacts and edges of the CNT, and the results are then representative of the CNT field emission.

problem. Since only one large scale eigenvalue problem and a small number of reduced eigenvalue problems need to be solved by time intervals, the computational efficiency and time savings offer by BTPS are significant.

It is straightforward to note that the direct scheme can also be used to address self-consistent TDDFT calculations using the adiabatic local density approximation (ALDA) where the potentials v_H and v_{xc} (5) need to be calculated at each time step in function of the local density. In order to take advantage of the BTPS scheme for interacting systems, however, one would need to adequately keep track of the variation of the density self-consistently with the local potential by considering a small enough time interval Δ_t . Since density and potential are likely to exhibit much weaker variations with time as com-

pared to individual wave functions, BTPS should still provide significant computational time savings as compared to the direct approach.

To summarize, the spectral-based propagation schemes proposed here with in particular the optimized BTPS approach, are potentially capable to open new perspectives in time dependent simulations of large-scale quantum systems. Possible applications of these techniques range from obtaining accurately the excited states of arbitrary molecules and nanostructures, to efficient characterization of high frequency responses of emerging nano-electronic materials and devices.

Acknowledgments

The authors wish to acknowledge helpful discussions with Dr. Sigfrid Yngvesson. This material is based upon work supported by the National Science Foundation: Grants No. ECCS 0725613, and No ECCS 0846457.

-
- [1] K. Fu, R. Zannoni, C. Chan, S. Adams, J. Nicholson, E. Polizzi, and K. Yngvesson, *Applied Physics Letters* **92**, 033105 (2008).
 - [2] T. Iitaka, *Physical Review E* **49**, 4684 (1994).
 - [3] A. Castro, M. Marques, and A. Rubio, *Journal of Chemical Physics* **121**, 3425 (2004).
 - [4] J. Crank and P. Nicolson, *Advances in Computational Mathematics* **6**, 207 (1996).
 - [5] T. Mikhailova and V. Pupyshchev, *Physics Letters A* **257**, 1 (1999).
 - [6] O. Sugino and Y. Miyamoto, *Physical Review B* **59**, 2579 (1999).
 - [7] A. Bandrauk and H. Shen, *The Journal of Chemical Physics* **99**, 1185 (1993).
 - [8] E. Polizzi, *Physical Review B* **79**, 115112 (2009).
 - [9] E. Polizzi, *The FEAST eigenvalue solver* (2009), URL <http://www.ecs.umass.edu/~polizzi/feast>.
 - [10] E. Runge and E. Gross, *Physical Review Letter* **52**, 997 (1984).
 - [11] W. Kohn and L. Sham, *Physical Review* **140**, A1133 (1965).
 - [12] D. Zhang and E. Polizzi, *Journal of Computational Electronics* **7**, 427 (2008).

- [13] D. Zhang and E. Polizzi, 13th International Workshop on Computational Electronics, (IWCE) proceedings pp. 1–4 (2009).
- [14] A. Mayer, Carbon **42**, 2057 (2004).